

# A new hypothesis for the deep subsurface structures near the Bhuj 2001 earthquake ( $M_w$ 7.6) hypocentre zone and its tectonic implications

E. Chandrasekhar,<sup>1</sup> George Mathew<sup>1</sup> and T. Harinarayana<sup>2</sup>

<sup>1</sup>Department of Earth Sciences, Indian Institute of Technology Bombay, Powai, Mumbai 400076, India. E-mail: esekhar@iitb.ac.in

<sup>2</sup>National Geophysical Research Institute, Hyderabad 500007, India

Accepted 2012 April 30. Received 2012 April 5; in original form 2012 January 18

## SUMMARY

We provide a new hypothesis for the deep subsurface structures near the Bhuj 2001 earthquake region based on magnetotelluric (MT) investigations carried out close to the epicentre zone. 2-D inversion of broad-band MT data of two profiles of lengths 32 km (AA') and 52 km (BB') revealed a thick (~3 km) highly conductive (1–4  $\Omega$ -m) surface layer of fluvio-marine Mesozoic–Cenozoic sediments. The models delineate the hypocentre zone located at ~20–25 km depth that manifests the high resistivity–conductivity transition zone. The accumulation of compressive stresses post-rifting along this weak zone has resulted in the reverse slip of Bhuj 2001 earthquake. The reverse fault ( $F_1$ ) associated with the earthquake is believed to be an ancient normal fault formed during the rifting phase. Contrary to earlier suggested theories, we suggest that  $F_1$  got initiated along the high resistivity–conductivity transition zone causing the Bhuj 2001 event. The geoelectric models revealed a laterally extending partially resistive zone at 20–30 km depth range showing a tendency to extend further deep. Model calculations using synthetic data also support this observation. Therefore, we hypothesize the presence of a basal detachment, marking the transition zone between the continental crust and the lithospheric upper mantle at ~40 km depth, intersected by the  $F_1$ . The geoelectric models suggest that the crustal thinning caused the asthenospheric upwelling and/or serpentinization leading to the ascent of volatiles and melts. The subsurface geometry in Kachchh basin suggests the thick-skinned deformation.

**Key words:** Magnetotelluric; Seismicity and tectonics; Continental tectonics: compressional; Asia.

## 1 INTRODUCTION

The Kachchh basin in Western India is tectonically active and lies in the zone of highest seismic risk, designated as 'Zone V' by the India Meteorological Department (IMD 2002). It has a history of continuous moderate-to-large seismicity including the two devastating continental intraplate earthquakes of 1819 (the Allahbund earthquake,  $M_w = 7.8$ ) and 2001 (Bhuj earthquake,  $M_w = 7.6$ ; Karanth *et al.* 2001; Biswas 2005; Mathew *et al.* 2006). The Kachchh Mainland Fault (KMF) is believed to be the principal active fault that controls the geometry of the basin (Fig. 1a). The eastern flank of KMF lies close to the South Wagad Fault (SWF), where the transpressional stresses between KMF and SWF are believed to have caused many earthquakes in the strained eastern part of the basin (Biswas 2005; Mathew *et al.* 2006; Mallik *et al.* 2008). The deep (~10–25 km) crustal intraplate seismicity in most continental rift regions is often attributed to strain accumulation aided by mafic intrusive bodies and hydrous melts in the hypocentre zones (Pollitz *et al.* 2002; Tank

*et al.* 2005). Crustal intrusive structures in Bhuj region have been delineated by earthquake tomography (Kayal *et al.* 2002), gravity and magnetic studies (Chandrasekhar & Mishra 2002) and by seismic refraction studies (Reddy 2005). Passive seismological studies have indicated fluids at lower crustal depths (20–30 km; Mishra & Zhao 2003). Biswas (2005) also suggested the presence of a large magmatic body in the deeper crust formed by lithosphere melting. Mandal *et al.* (2004) considered an unknown fault, the North Wagad Fault (NWF) to be the causative structure for the Bhuj earthquake. However, Mathew *et al.* (2006) suggested a hidden South Wagad Master Fault beneath the Wagad zone as the causative fault. Although most previous studies argue that the Bhuj earthquake was aided by fluids at lower crustal depths, the cause for the 2001 Bhuj event remains enigmatic. This is largely due to insufficient geophysical data to reliably constrain the subsurface structure near the hypocentre zone.

Magnetotelluric (MT) investigations provide complementary information by characterizing the subsurface electrical conductivity as

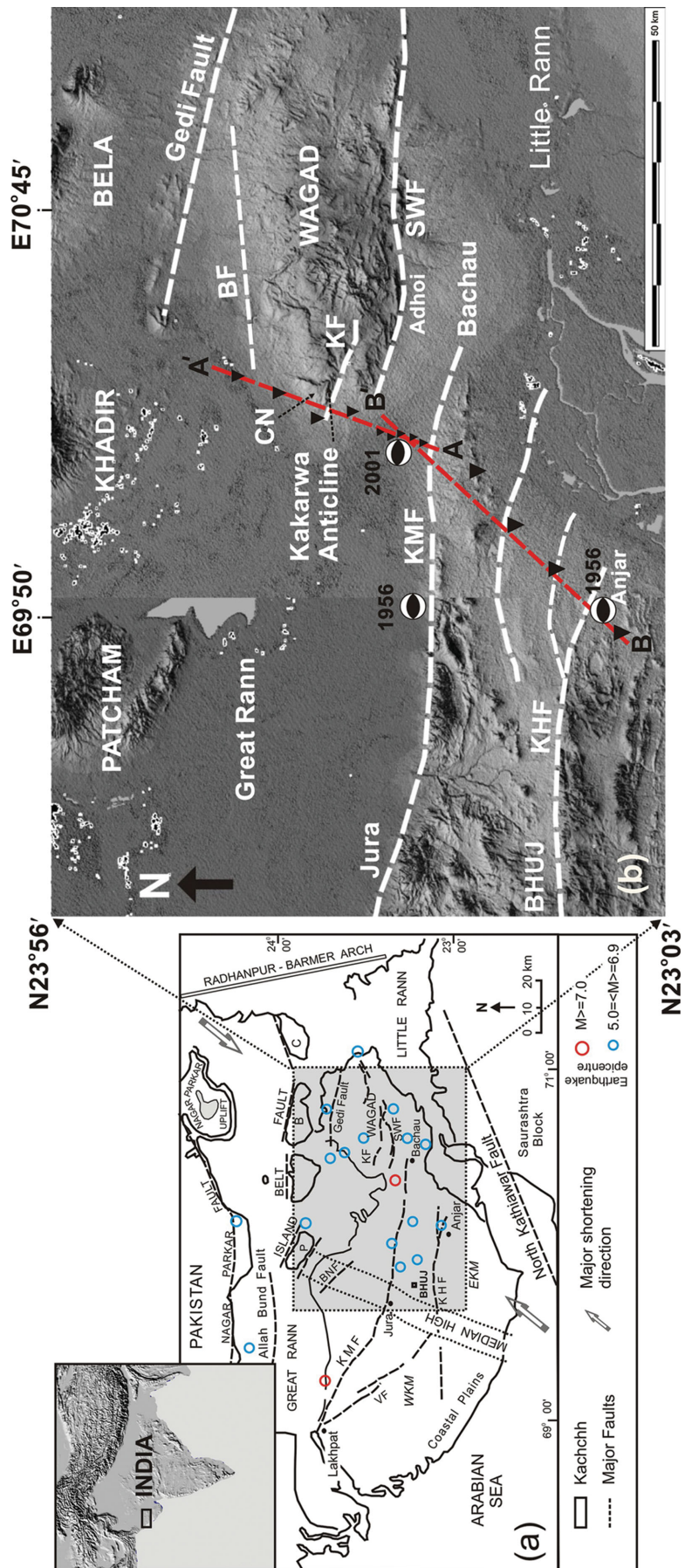


**Figure 1.** (a) Geographical location of MT stations superposed on a seismotectonic map of Kachchh region, whose data are used in this study. Epicentre locations of various major and minor seismic events are also shown. KMF, Kachchh Mainland Fault; KHF, Katrol Hill Fault; VF, Vigodi Fault; BNF, Banni Fault; SWF, South Wagad Fault; P, Pachham Island; BF, Bharodia Fault; CN, Chobari Nose; K, Khadir Island; B, Bela Island; C, Chorar Island; KF, Kanthkot fault; EKM, Eastern Kachchh Mainland; WKM, Western Kachchh Mainland (after Biswas 2005; Mathew *et al.* 2006). (b) Geographical location of the MT stations superposed on a SRTM Digital elevation model (DEM) of the Kachchh region in western India, having 90 m spatial resolution.

diagnostic tool. Sastry *et al.* (2008) and Naganjaneyulu *et al.* (2010) have carried out MT studies across a variety of fault structures in the western and central Kachchh basin. Although their investigations reveal high resistive bodies in the lower crustal depths separated by conductive zones, their study lacked adequate information to deduce a probable cause for the Bhuj 2001 event. This is because, their profiles were not close to the epicentre zone and the sites were also widely spaced.

Knowledge of the basin architecture and lithology near the hypocentre zone is very important to clearly understand the reasons for the occurrence of the Bhuj 2001 event. In this study, we analyse wide-band MT data from two profiles, AA' and BB' (Fig. 1b) and attempt to understand the overall nature of subsurface geometry around the hypocentre zone and infer the tectonic implications. The AA' profile is ~32 km in length, with closely spaced station intervals and is located close to the epicentre zone at the eastern end of KMF, crossing SWF. The other profile BB' has a length of ~52 km and partially overlaps with AA'. The organization of the paper is as follows. We first discuss the geology of the Kachchh region followed by MT data acquisition, processing and 2-D inversion. Finally, we discuss the tectonic interpretation of the delineated geoelectrical resistivity models.

## 2 GEOLOGICAL SETTING

The Kachchh region in the western India is widely considered to be the largest and the earliest intracontinental rift basin. The rifting was initiated during the separation of the Indian Plate from Gondwana. The basin consists largely of four lithologies: the Precambrian felsic basement, Jurassic-Cretaceous sandstones, Deccan volcanic rocks and the Tertiary-Quaternary sediments (Biswas 2005). Basin inversion began after the onset of subduction of the Indian Plate beneath the Eurasian Plate during the Middle-Late Tertiary, resulting in the reactivation of normal faults and the formation of reverse faults. The KMF and the SWF are the two examples of reverse movement along the pre-existing normal fault planes that resulted in development of anticlines in the overlying Mesozoic sandstone. The hinges of the anticlines are completely eroded forming topographic depressions (Mathew *et al.* 2006; Mallik *et al.* 2009). The general trends of reverse faults are E-W. The KMF is ~120 km long and marks the boundary between the Kachchh mainland and the Quaternary sediments of the Great Rann and the Banni plains (Fig. 1a). The other major faults in the region are the Nagar Parkar Fault (NPF), the Allahbund Fault, the Island Belt Fault, the Banni Fault (BNF) and the Katrol Hill Fault (KHF; Fig. 1a). The Kachchh rift is bounded by the NPF to the north and by the North Kathiawar fault to the south. The Radhanpur-Barmer arch bounds the rift to the east. The rift terminates in the continental shelf towards the west. Mesozoic, Tertiary and Quaternary sediments fill up the basin. The sediment thickness varies from <2 km in the north to >4 km in the south and from 200 m in the east to >2.5 km in the west. The exposed geology in the epicentre zone consists of recent sediments on a flat terrain with nothing to indicate subsurface deformation. Since the 2001 event had occurred on a blind fault, it produced only secondary deformational features (Karanth *et al.* 2001).

## 3 MT DATA ACQUISITION AND PROCESSING

In 2009 and 2010, wide-band five-channel MT data were recorded at nine stations along AA' profile using the ADU07 instrument of

Metronix GmbH. This profile lies close to the epicentre zone at the eastern end of KMF, crosses SWF and extends up to south of Gedi Fault (Fig. 1b). Fig. 1(b) depicts the SRTM-digital elevation model (DEM) having a spatial resolution of 90 m. Magnetic field measurements were made using MFS06 coils and the electric field measurements were made using Pb-PbCl<sub>2</sub> electrodes. The E-W and N-S electrode separation was maintained 40 m at each site. Data were recorded at each site for about 30–35 hr spanning the period range of 0.001–1000 s. The low cultural and industrial noise in this part of study region has resulted in high quality data. However, the MT dead-band noise (that arises usually due to the cross-over frequencies between ionospheric induced energy and lightning induced energy) has contaminated the data at a couple of stations near the northern end of the profile. Data were processed with MAPROS software using the spectral stacking algorithm of Junge (1996) to determine the apparent resistivity and phase estimates.

Five MT stations from the AA' profile were joined with the available MT data from four more stations (MB05, MB06, KB08 and KB15) located SW to AA' to form another profile, BB' (Fig. 1b). Data at the latter four stations were recorded in 2006 using the ADU06 instrument of Metronix GmbH. These data were processed following the procedure described earlier. There are large gaps between the stations of profile BB'. Our recent attempts to fill these gaps, particularly between MB05 and MB06 were not successful due to the high-tension power lines that have recently been built.

### 3.1 Strike angle estimation and static shift correction

Following the procedure outlined by Groom *et al.* (1993) we have decomposed the MT impedance tensor elements to constrain the galvanic distortion parameters: shear, twist and strike (Groom & Bailey 1989). This was done using the 'strike' program of McNeice & Jones (2001). The procedure that we have adopted to determine the strike angle is detailed in Chandrasekhar *et al.* (2009b). Within the period range from 0.001 to 1000 s, the unconstrained twist (shear) values are  $\pm 5^\circ$  ( $\pm 25^\circ$ ) for AA' stations located close to epicentre region. The existence of significant shear values even at >100 s at some stations of both profiles suggests that the deep-rooted inhomogeneities are responsible for causing the frequent earthquakes in the tectonically active Kachchh region. The period range mentioned earlier was used for determining the strike angle along both profiles. The mean strike angle is  $-75^\circ$  ( $-65^\circ$ ) for the AA' (BB'), which is in agreement with that obtained for the Kachchh region by Sastry *et al.* (2008). Fig. 2 shows the Rose diagrams depicting the individual strike angles obtained for the AA' (Fig. 2a) and BB' (Fig. 2b) profiles. The MT impedance tensors corresponding to both profiles were rotated by the respective strike angles prior to further processing. Consistent with the fact that static shift effects are less significant in conductive environment (Simpson & Bahr 2005), static shift effects in the AA' and BB' data are not significant, since the entire Kachchh basin is filled with high conductive marine sediments. The minor static shifts were corrected by comparing the apparent resistivity values of adjacent stations (Christopherson *et al.* 2002) before implementing the 2-D inversion scheme.

### 3.2 Two-dimensional inversion

2-D inversion of MT data of the AA' profile in the period range 0.001–1000 s was carried out using the non-linear conjugate

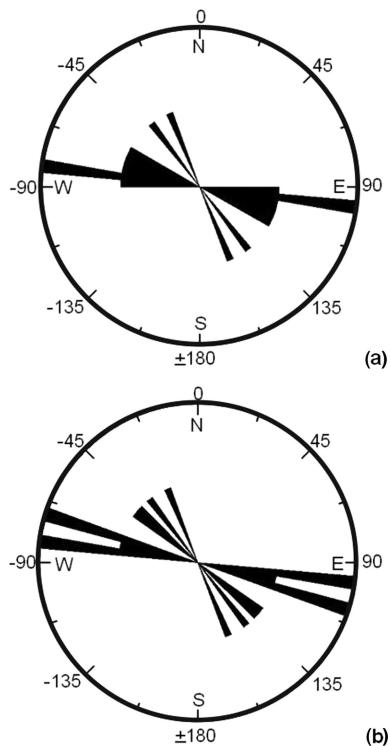


**Figure 2.** Rose diagrams depicting the strike angles, corresponding to the stations of (a) AA' and (b) BB' profiles.

gradient algorithm of Rodi & Mackie (2001). We have jointly inverted the TE and TM mode apparent resistivity and phase data with error floors of 10 per cent on apparent resistivity and 5 per cent on phase. The smoothing factor ( $\tau$ ) was set at 3.  $\tau$  indicates the trade-off between the data misfits and the model smoothness. Larger values of  $\tau$  results in smoother models, but at the expense of a poorer fit between the data and the model. Rodi & Mackie (2001) suggest that  $\tau$  can be set in the range of 3–300. However, it should optimally be so chosen, that the rms error between the data and model be 1.0 and 1.5. Since we wanted to have as much best fit as possible between the data and model, we have set  $\tau$  at its lowest value, 3. Fig. 3 shows the fit between data and model response for a few selected stations of both profiles together with their respective rms errors. Fig. 4(a) shows the resulting geoelectrical model with an rms error of 1.04. A high conductive thin ( $\sim 2$  km) surface layer is present along the entire profile. The hypocentre location at  $\sim 20$ – $25$  km depth signifying the transition zone  $F_1$ , separates the high-resistive lithology ( $R_1$ ) and the adjacent conductive zone.

Fig. 4(b) shows the geoelectrical model corresponding to BB' profile with rms error 1.46, obtained by using the same inversion parameters as used in case of AA'. The sharp resistivity contrast along the hypocentre axis is also clearly seen in Fig. 4(b). The large-scale resistive structure extending to 20–30 km depths could be an extension of  $R_1$ , showing a tendency to extend even below 30 km depth. To validate the presence of this feature, we have made further model calculations using synthetic data with 15 per cent of Gaussian noise added. Synthetic data were generated for 25 closely spaced sites (16 new sites and existing 9 sites of BB' profile) using the following model: (i) a highly conductive surface layer ( $1$ – $4 \Omega\text{-m}$ ) of 4 km thickness, (ii) a high resistive block ( $6500 \Omega\text{-m}$ ) (representative of  $R_1$ ) with dimensions 15 km by 16 km buried at depth of 4 km, starting from the midpoint of KB08 and

KB15 and extending up to SW03, (iii) a deeper resistive block ( $1600 \Omega\text{-m}$ ) of dimensions  $28 \text{ km} \times 24 \text{ km}$  buried at 22 km depth starting from the southern end of the profile and (iv) a very high conductive zone ( $1$ – $4 \Omega\text{-m}$ ) of dimensions  $9.5 \text{ km} \times 12 \text{ km}$  (representative of  $C_2$ ) buried at a depth of 4.5 km and located between the stations MB06 and KB08. The background resistivity of the model is set at  $100 \Omega\text{-m}$ . Inversion parameters for modelling synthetic data are also same as those set for real data. Inversion results of synthetic data indicate the possible presence of a laterally extending large resistive body at 25–40 km depth. The resolution of this feature is poor and diminishes with depth due to the very high conductive surface layer, as is the case with the real data also. On the other hand, removal of this feature from the model largely increased the misfit between the data and the model, suggesting that the model requires this feature to support the real data.

#### 4 RESULTS AND DISCUSSION

Inversion results of AA' shows a highly conductive ( $1$ – $4 \Omega\text{-m}$ ) surface layer of  $\sim 2.0$ – $2.5$  km thickness interpreted as fluvio-marine Mesozoic-Cenozoic sandstones and sediments. Interconnected saline fluids in the porous surficial sediments account for high conductivity (Palacky 1991). The model also reveals a high resistive body ( $R_1$ ;  $1000$ – $6000 \Omega\text{-m}$ ) at mid-crustal depths, with resistivity gradation extending up to  $\sim 30$  km depth and curving southward at greater depths. The transition zone between the resistive and conductive lithologies along the hypocentre axis may have acted as the surface for the reverse slip associated with the great Bhuj earthquake. This transition zone is termed as Fault Zone Conductor (FZC). Hypocentres of many earthquakes are located in the FZC zones, characterized by the high resistivity contrast between two adjacent subsurface blocks (Unsworth & Bedrosian 2004; Tank *et al.* 2005; Chen *et al.* 2007).

We suggest that  $R_1$  represents the unfractured Pre-Cambrian felsic crust, while the conductive zone represents the altered and metasomatised crust. Fault plane solutions for the Bhuj event indicate that the hypocenter lies in the depth range 17–24 km with a dip of  $45^\circ$  due south (Negishi *et al.* 2001). Comparison of seismological data with MT inversion results associates the fault with the transition zone. Accordingly, we define the thrust fault,  $F_1$  (Figs 4a & b). Thus we propose that the Bhuj earthquake had occurred due to the reverse movement along  $F_1$ . Prior to the earthquake,  $F_1$  was probably a high angle, thick-skin normal fault that developed initially during the rifting phase of the Kachchh basin. The transition zone at the hypocentre location thus constituted a weak zone between the resistive and high conductive lithologies.  $F_1$  appears to cut across the basement crust and perhaps joins a low angle ramp of the underlying basal detachment, probably located below 35 km depth. The detachment marks the transition zone between the continental crust and the lithospheric upper mantle. We suspect this could be the laterally extending resistive structure near the Moho discontinuity at 35–40 km depth (Fig. 4b). The resistive structure  $R_1$  curves southward below 30 km depth and might also join the detachment. However, it is unclear, if the lithologies of  $R_1$  and the resistive basal detachment are the same. The resistivity of the basal detachment could not be clearly resolved due to the very high conductive surface layer as also confirmed by model calculations using synthetic data. The deep resistive structure in Kachchh is further corroborated by the observed high velocity lower crust in the seismically active Anjar-Bachau region, as deduced by single-fold seismic reflection data (Reddy *et al.* 2001). Naganjaneyulu *et al.* (2010) placed the

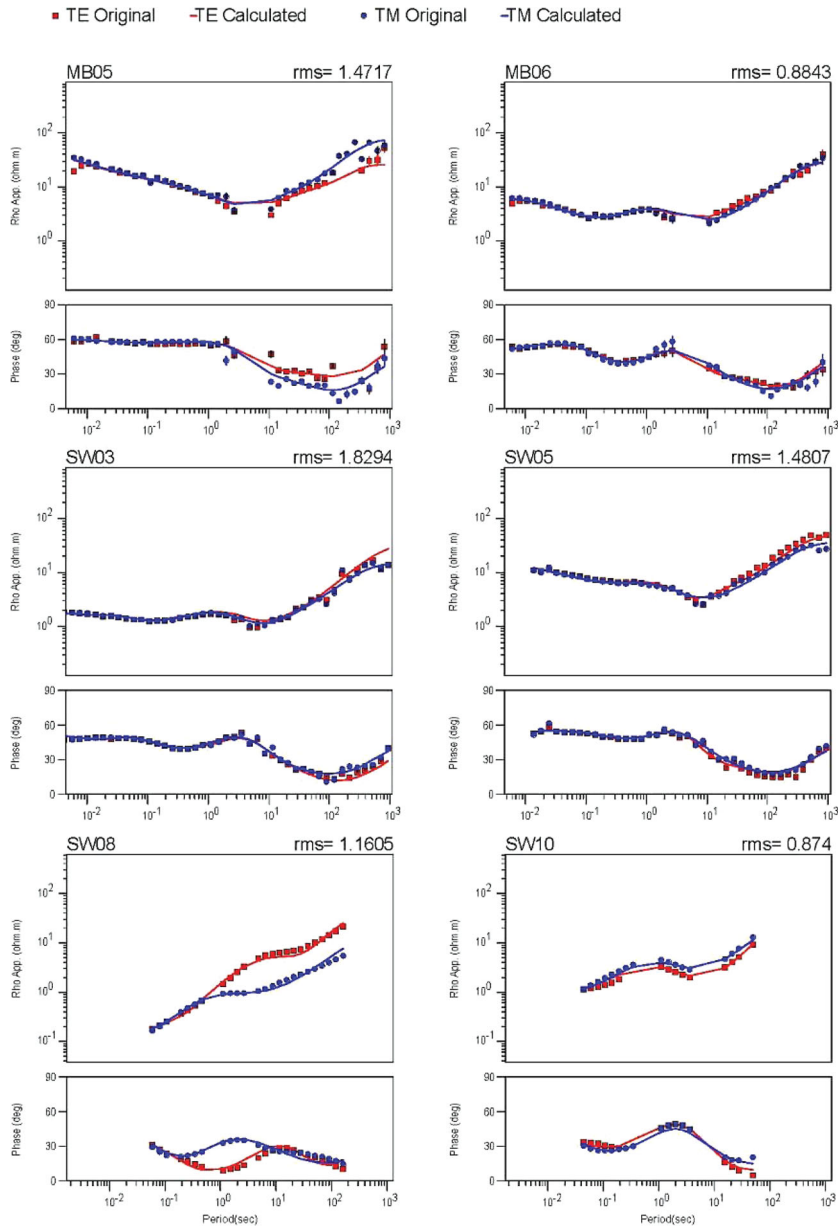


**Figure 3.** Comparison between the observed data and their corresponding modelled responses of TE and TM modes at some of the selected stations shown in Fig. 4.

Moho at a depth 35–40 km below the hypocentre zone, while the Moho at Anjar (see Fig. 1) is indicated below 45 km depth. Similarly, Mandal (2011) suggests a transitional Moho in the 34–42 km depth range, indicating the presence of an ultramafic intrusion. These observations led us to argue strongly for the basal detachment zone as shown in Fig. 4, formed during the rifting phase. All crustal-scale normal faults, after refraction in the underlying ductile zone, probably culminated at the detachment zone. Seismic tomography studies in Kachchh region have mainly focused on discussing the nature of subsurface around the hypocentre zone of the 2001 event and the aftershock velocity pattern in the Kachchh region (see Mandal & Rodkin 2011 and the references therein). These studies did not interpret the fault geometry and the associated tectonism on the lines of basal detachment that we propose here.

Resistivity contrasts observed in the conductive sedimentary upper crust are interpreted as faults and marked as  $F_2$  and  $F_3$  (Fig. 4a).

The sedimentary units on either side of  $F_2$  are elevated 0.5 km above the resistive block  $R_1$ . Similarly,  $F_3$  is interpreted to be the bounding fault of the Kakarwa anticline, the Kanthkot Fault (KF; Fig. 1b). The zone closest to Kakarwa anticline is called Chobari Nose (CN; Fig. 1b), owing to the shape of the topography in the eastern Wagad region (see Fig. 1b). Note the deep crustal conductive zone  $C_1$  (Fig. 4a) ascending into the upper sedimentary crust near the station SW09. The presence of saline fluids in the mid to lower crust is expected to reduce the resistivity. However, their presence from below 30 km indicates probable ascent of partial melts due to the asthenosphere upwelling and/or serpentinization of the upper mantle. Further, the possibility of percolation of marine water in the upper zone cannot be ruled out due to the proximity of the brittle upper crust. The fault  $F_4$  representing the transition zone between the conductive and resistive lithologies could be the signature of Bharodia Fault (BF; see Fig. 1b). The resistive zone north of SW10

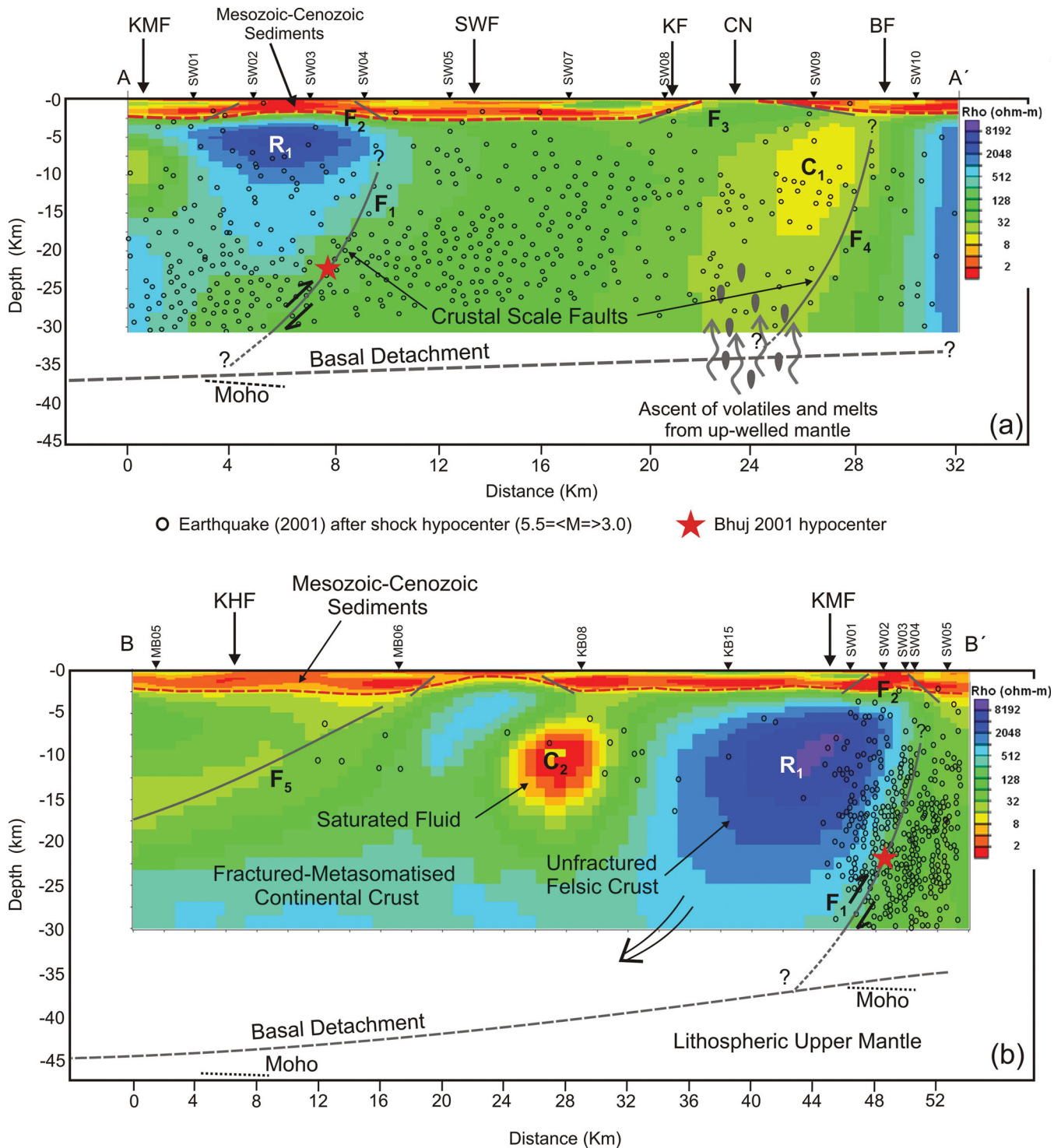


**Figure 4.** (a) 2-D model of MT data of nine stations corresponding to AA' profile (Fig. 1b). The model is obtained after jointly inverting the TE and TM mode data with an error floor of 10 per cent (5 per cent) for apparent resistivity (phase) by setting the smoothing parameter  $\tau$ , at 3 (Rodi & Mackie 2001). The rms error for model is 1.04. F<sub>1</sub> and F<sub>4</sub> depict the possible crustal-scale faults, representing the subsurface high conductivity-resistivity transition zones. F<sub>2</sub> and F<sub>3</sub> depict the small-scale hidden faults. The surface manifestations of Choubari Nose (CN) and Bharodia Fault (BF) are also clearly seen. C<sub>1</sub> represents the zone of partial melts due to asthenosphere upwelling and/or serpentinisation of the upper mantle. (b) 2-D model of MT data of nine stations along the BB' profile (Fig. 1b). Inversion parameters for this model are same as those of (a). The rms error for model is 1.46. The model clearly maps the hidden faults, F<sub>1</sub>, F<sub>2</sub> and F<sub>5</sub> (see text for details). Distribution of small open circles superposed on both the models represents the hypocentres of many earthquakes occurred in this region. These are not magnitude-classified. The numbering of faults in both models is done arbitrarily and does not bear any relation with their geological age.

station is an artefact of the model. However, if this zone were actually resistive, then it could be another high conductivity–resistivity transition zone. The resulting weak  $F_4$  zone could trigger a future seismic event, as the geoelectrical nature around  $F_4$  is similar to that around  $F_1$ . Further MT recordings north of SW10 are required to substantiate this idea.

Fig. 4(b) also shows a highly conductive surficial layer of fluvio-marine Mesozoic–Cenozoic sediments with thickness varying from 2.5 km in the north to 3 km in the south. The resistive body  $R_1$  could have escaped the rift-related intense fracturing and the later metasomatism by the upwelling melts and volatiles. The basaltic volcanism (Deccan) during the Late Cretaceous also does not seem to have influenced the geoelectrical structure of the subsurface, although major basalt exposures are largely confined to the south of Bhuj city. The crust at the depth 4–20 km beneath the southern end of BB' profile, includes a conductive zone (8–30  $\Omega$ -m), interpreted as fractured felsic crust saturated with fluids. The thicker high conductive zone beneath MB05 gradually thins towards MB06 along the fault,  $F_5$  (Fig. 4b), whose surface manifestation is interpreted to be a branch of the KHF (see Fig. 1b), formed under compressive stresses. The basement reverse fault seems to have also inverted the rift-bounding normal fault in the sedimentary layers. Present MT data cannot delineate KHF, perhaps due to the large station gap between the sites MB05 and MB06.

The localized high conductive feature ( $\sim$ 1–8  $\Omega$ -m) seen at 5–18 km depth beneath KB08 ( $C_2$ ; Fig. 4b) is interpreted to be a zone, saturated with saline fluids. The fluids seem to have fed from the surface since  $C_2$  appears to extend into the top sedimentary layer. We have tested the veracity of  $C_2$  by modelling the data with and without  $C_2$ . We find that the data fits well with the model when  $C_2$  is present (rms = 1.46) than not (rms = 1.7). Model calculations using synthetic data also suggest the need for  $C_2$  to support the data. Further, seismic refraction studies by Prasad *et al.* (2010) also have revealed that the  $C_2$  has low velocities. The topography in this zone shows curved ridges of sandstone, rich in hydrothermal iron alterations and desilicification. If  $C_2$  were to be a zone of interconnected aqueous fluids, then the situation is consistent with the thick-skinned deformation. Similar observations on the release of fluids at mid-crustal depths from prograde metamorphism were attributed to the thick-skinned deformation in South Island of New Zealand (Wannamaker *et al.* 2002) and in Taiwan (Bertrand *et al.* 2009).

Based on the analyses of data from the AA' and BB' profiles, we hypothesize that continental extension resulted in extensive fracturing of the Precambrian crust, and the development of a detachment fault cutting through the crust and upper mantle, resulting in the generation of mantle shear zone below  $\sim$ 40 km depth. Significant lithospheric thinning would have resulted in asthenosphere upwelling and melting and upward ascent of volatile rich melts accompanied by metasomatism of the crust. Several plugs of alkali basalts in Kachchh contain spinel peridotite xenoliths of mantle origin (Karmalkar *et al.* 2005). The clinopyroxene rare earth element data from the region suggest partial melting of the primitive mantle source material in the spinel peridotite field (Karmalkar *et al.* 2005).

Fracturing of the lower crust during the rifting phase might have also allowed penetration of water into the mantle beneath the brittle crust. This could have resulted in serpentinization of the upwelling upper mantle (Reston *et al.* 2001). The volume increase accompanying serpentinization caused local uplift of the overlying crust and extension then becoming more focused above the serpentinization region. Continued serpentinization during further extension and mantle

unroofing increased the volume of serpentinites and reduced their density to an extent that could have caused diapirism. The serpentine diapirs may have followed zones of structural weakness to penetrate the overlying crustal sections between fault blocks ( $F_4$  in Fig. 4a). Chandrasekhar *et al.* (2009a), based on a six-year observation of GPS deformation rates, report unusually low viscosity of the mantle below the Bhuj earthquake epicentral zone, attributed to the thermal weakening and hydration of the mantle. High pore-fluid pressure plays an important role in lubricating the fault planes, thereby assisting thrust faulting. We believe that the fault  $F_4$  was formed initially during the rifting phase. The crustal thinning resulted in asthenospheric upwelling, and/or serpentinization, leading to the ascent of volatiles and melts (Fig. 4a).

The compressive forces due to rift inversion have converted the fault  $F_1$  to a reverse fault during the Bhuj 2001 event. The broad, diffused aftershock pattern around the hypocentre indicate that the  $F_1$  reversal could have triggered movements on the underlying basal detachment fault, resulting in movement and later relaxation on other faults, particularly those that constitute a weak zone between electrically contrasting lithologies.

Through the above interpretation, we have provided a demonstrable evidence that the reverse fault  $F_1$  is mainly responsible for the Bhuj 2001 event. Mandal *et al.* (2004) suggested the unknown NWF, which actually lies  $\sim$ 2 km north of station SW10, as the causative fault responsible for Bhuj 2001 event. However, for the NWF to be the causative fault, it must extend almost  $\sim$ 30 km from the epicentre location (see Fig. 1b) and cut across several mapped faults, shown in Fig. 4. If such a large fault had really existed, our MT data would have shown relevant signature beneath SW05, SW07 and SW08, particularly as station spacing in this part of the profile is relatively close. Since no feature of any extending fault is seen beneath these stations (Fig. 4a), we do not support the hypothesis of NWF. Therefore, in the light of the dense distribution of the 2001 aftershock pattern and the hypocentre location of the main shock, the mapped reverse fault,  $F_1$ , associated with the high resistivity–conductivity transition zone along the hypocentre axis, is suggested to be the main causative fault responsible for the Bhuj 2001 event.

## 5 CONCLUSIONS

The geoelectric models corresponding to AA' and BB' MT profiles have revealed various hidden faults, on which several earthquakes of different magnitudes have occurred. The crustal-scale reverse fault,  $F_1$ , is suggested herein, to be the causative fault responsible for the devastating Bhuj 2001 event, dismissing the earlier reported NWF. The resistive–conductive transition zone along the hypocentre axis was a pre-existing zone of weakness that initially developed as a normal fault during the rifting phase of the Kachchh basin. Later, compressive forces along this zone of weakness resulted in reverse slip at the transition zone. We hypothesize the existence of a basal detachment, marking the transition zone between the continental crust and the lithospheric upper mantle, intersected by the mapped reverse fault. The crustal-scale fault  $F_4$  (BF; Fig. 4a), located close to the northern end of AA' profile reveals upwelling of the melts and volatiles. BF was probably initiated from the basal detachment zone during the rifting phase. This zone shows a second high conductive–resistive transition zone, which could be liable for future slip due to the ongoing compressive stresses, leading to an impending future earthquake. The subsurface geometry in Kachchh basin suggests the thick-skinned deformation.

## ACKNOWLEDGMENTS

EC thanks the Ministry of Earth Sciences, Govt. of India for financial support and IIT Bombay for procuring the ADU07 MT unit. We sincerely thank Dr. Heinrich Brasse for some helpful discussions on the modelling aspects. GM acknowledges the funding provided by the Department of Science and Technology (DST, Govt. of India, New Delhi) under the Shallow Subsurface Science project. The authors thank the editor Dr. Mark Everett and two anonymous reviewers for improving the paper with their constructive comments. The authors acknowledge the support of Ms. Padmasri Morri, Mr. Rajesh, Mr. Deepak Gosai and Mr. Salim Jumma for their help in the field.

## REFERENCES

- Bertrand, E. *et al.*, 2009. Magnetotelluric evidence for thick-skinned tectonics in central Taiwan, *Geology*, **37**, 711–714, doi:10.1130/G25755A.1.
- Biswas, S.K., 2005. A review of structure and tectonics of Kutch basin, western India, with special reference to earthquakes, *Current Sci.*, **88**, 1592–1600.
- Chandrasekhar, D.V. & Mishra, D.C., 2002. Some geodynamic aspects of Kachchh basin and seismicity: an insight from gravity studies, *Current Sci.*, **83**, 492–498.
- Chandrasekhar, D.V., Burgmann, R., Reddy, C.D., Sunit, P.S. & Schmidt, D.A., 2009a. Weak mantle in NW India probed by geodetic measurements following the 2001 Bhuj earthquake, *Earth planet. Sci. Lett.*, **280**, 229–235.
- Chandrasekhar, E., Fontes, S.L., Flexor, J.M., Rajaram, M. & Anand, S.P., 2009b. Magnetotelluric and aeromagnetic investigations for assessment of groundwater resources in Parnaiba basin in Piauí State of North-East Brazil, *J. appl. Geophys.*, **68**, 269–281, doi:10.1016/j.jappgeo.2008.12.001.
- Chen, C.C., Chi, S.C., Chen, C.S. & Yang, C.H., 2007. Electrical structures of the source area of the 1999 Chi-Chi, Taiwan, earthquake: spatial correlation between crustal conductors and aftershocks, *Tectonophysics*, **443**, 280–288, doi:10.1016/j.tecto.2007.01.018.
- Christopherson, K.R., Jones, A.G. & Mackie, R.L., 2002. Magnetotellurics for natural resources: from acquisition through interpretation, Soc. Explor. Geophys. Lecture Notes (unpublished).
- Groom, R.W. & Bailey, R.C., 1989. Decomposition of the magnetotelluric impedance tensor in the presence of local three-dimensional galvanic distortions, *J. geophys. Res.*, **94**, 1913–1925.
- Groom, R.W., Kurtz, R.D., Jones, A.G. & Boerner, D.E., 1993. A quantitative methodology for determining the dimensionality of conductivity structure from magnetotelluric data, *Geophys. J. Int.*, **115**, 1095–1118.
- IMD, Ministry of Earth Sciences, Government of India, Seismic Zoning Map, 2002, available at: <http://www.imd.gov.in/section/seismo/static/seismo-zone.htm> (last accessed 2012 April 4).
- Junge, A., 1996. Characterization of and correction for cultural noise, *Surv. Geophys.*, **17**, 361–391.
- Karanth, R.V., Sohoni, P.S., Mathew, G. & Khadkikar, A.S., 2001. Geological observations on 26<sup>th</sup> January 2001 Bhuj earthquake, *J. Geol. Soc. India*, **58**, 193–201.
- Karmalkar, N.R., Regea, S., Griffin, W.L. & O'Reilly, S.Y., 2005. Alkaline magmatism from Kutch, NW India: implications for plume-lithosphere interaction, *Lithos*, **81**, 101–119.
- Kayal, J.R., De, R., Ram, S., Srirama, B.V. & Gaonkar, S.G., 2002. Aftershocks of the January 26, 2001 Bhuj earthquake and its seismotectonic implications, *J. Geol. Soc. India*, **59**, 395–417.
- Mallik, J., Mathew, G., Thomas, R. & Greiling, R.O., 2008. Determination of horizontal principal directions of stress and active faults in Kachchh (India) by Electromagnetic Radiation (EMR), *J. Geodyn.*, **45**, 234–245.
- Mallik, J., Mathew, G. & Greiling, R.O., 2009. Magnetic fabric analysis of Fault Propagation Folds in the Eastern Kachchh, Western India, *Tectonophysics*, **473**, 428–445.
- Mandal, P., 2011. Crustal and lithological thinning beneath the seismogenic Kachchh rift zone, Gujarat: implication toward the generation of the 2001 Bhuj earthquake sequence, *J. Asian Earth Sci.*, **40**, 150–161.
- Mandal, P. & Rodkin, M.V., 2011. Seismic imaging of the 2001 Bhuj Mw7.7 earthquake source zone: b-value, fractal dimension and seismic velocity tomography studies, *Tectonophysics*, **512**, 1–11.
- Mandal, P. *et al.*, 2004. Characterization of the fault system for 2001 Bhuj earthquake of Mw 7.7, *Tectonophysics*, **378**, 105–121.
- Mathew, G., Singhvi, A.K. & Karanth, R.V., 2006. Luminescence chronometry and geomorphic evidence of active fold growth along the Kachchh Mainland Fault (KMF), Kachchh, India: seismotectonic implications, *Tectonophysics*, **422**, 71–87.
- McNeice, G.W. & Jones, A.G., 2001. Multisite, multifrequency tensor decomposition of magnetotelluric data, *Geophysics*, **66**(1), 158–173.
- Mishra, O.P. & Zhao, D., 2003. Crack density, saturation rate and porosity at the 2001 Bhuj, India, earthquake hypocenter a fluid-driven earthquake?, *Earth planet. Sci. Lett.*, **212**, 393–405.
- Naganjaneyulu, K., Ledo, J.J. & Queralt, P., 2010. Deep crustal electromagnetic structure of Bhuj earthquake region (India) and its implications, *Geologica Acta.*, **18**, 83–97.
- Negishi, H., Mori, J., Sato, H., Singh, R.P. & Kumar, S., 2001. Aftershocks and slip distribution of main shocks – a comprehensive survey of 26<sup>th</sup> January 2001 earthquake (Mw 7.7) in the state of Gujarat, India, Research Report on Natural disasters, December 2001, 33–45.
- Palacky, G.J., 1991. Resistivity characteristics of geologic targets, in *Electromagnetic Methods in Applied Geophysics*, pp. 53–129, ed. Naibhigian, M., Society of Exploration Geophysicists, Tulsa, Oklahoma.
- Pollitz, F.F., Kellogg, L. & Burgmann, R., 2002. Sinking mafic body in a reactivated lower crust: a mechanism for stress concentration at the New Madrid Seismic zone, *Bull. seism. Soc. Am.*, **91**, 1882–1897.
- Prasad, B.R., Venkateswarlu, N., Prasad, A.S.S.R.S., Murthy, A.S.N. & Sateesh, T., 2010. Basement configuration of on-land Kutch basin from seismic refraction studies and modeling of first arrival travel time skips, *J. Asian Earth Sci.*, **39**, 460–469.
- Reddy, P.R., 2005. Crustal velocity structure of western India and its use in understanding intraplate seismicity, *Current Sci.*, **88**, 1652–1657.
- Reddy, P.R., Sarkar, D., Sain, K. & Mooney, W.D., 2001. A report on a collaborative scientific study at USGS, Melno Park, USA, 1–31.
- Reston, T.J., Pennel, J., Stuberndrauch, A., Walker, I. & Gussinye, M.P., 2001. Detachment faulting, mantle serpentinization, and serpentinite mud volcanism beneath the Porcupine Basin, southwest of Ireland, *Geology*, **29**, 587–590.
- Rodi, W. & Mackie, R.L., 2001. Nonlinear conjugate gradients algorithm for 2-D magnetotelluric inversion, *Geophysics*, **66**, 174–187.
- Sastry, R.S., Nagarajan, N. & Sarma, S.V.S., 2008. Electrical imaging of deep crustal features of Kutch, India, *Geophys. J. Int.*, **172**, 934–944, doi:10.1111/j.1365-246X.2007.03658.x.
- Simpson, F. & Bahr, K., 2005. *Practical Magnetotellurics*, Cambridge University Press, UK.
- Tank, B. *et al.*, 2005. Magnetotelluric imaging of the fault rupture area of the 1999 İzmit (Turkey) earthquake, *Phys. Earth planet. Inter.*, **150**, 213–225.
- Unsworth, M.J. & Bedrosian, P.A., 2004. On the geoelectric structure of major strike-slip faults and shear zones, *Earth Planets Space*, **56**, 1177–1184.
- Wannamaker, P.E., Jiracek, G.R., Stodt, J.A., Caldwell, T.G., Gonzalez, V.M., McKnight, J.D. & Porter, A.D., 2002. Fluid generation and pathways beneath an active compressional orogen, the New Zealand Southern Alps, inferred from magnetotelluric data, *J. geophys. Res.*, **107**, 2117, doi:10.1029/2001JB000186.